LBL-30418
Preprint

Lawrence Berkeley Laboratory
UNIVERSITY OF CALIFORNIA

Accelerator & Fusion Research Division

Submitted to Nuclear Instruments and Methods in Physics Research A

Standing-Wave Free-Electron Laser Two-Beam Accelerator

A.M. Sessler, D.H. Whittum, J.S. Wurtele, W.M. Sharp, and M.A. Makowski

February 1991

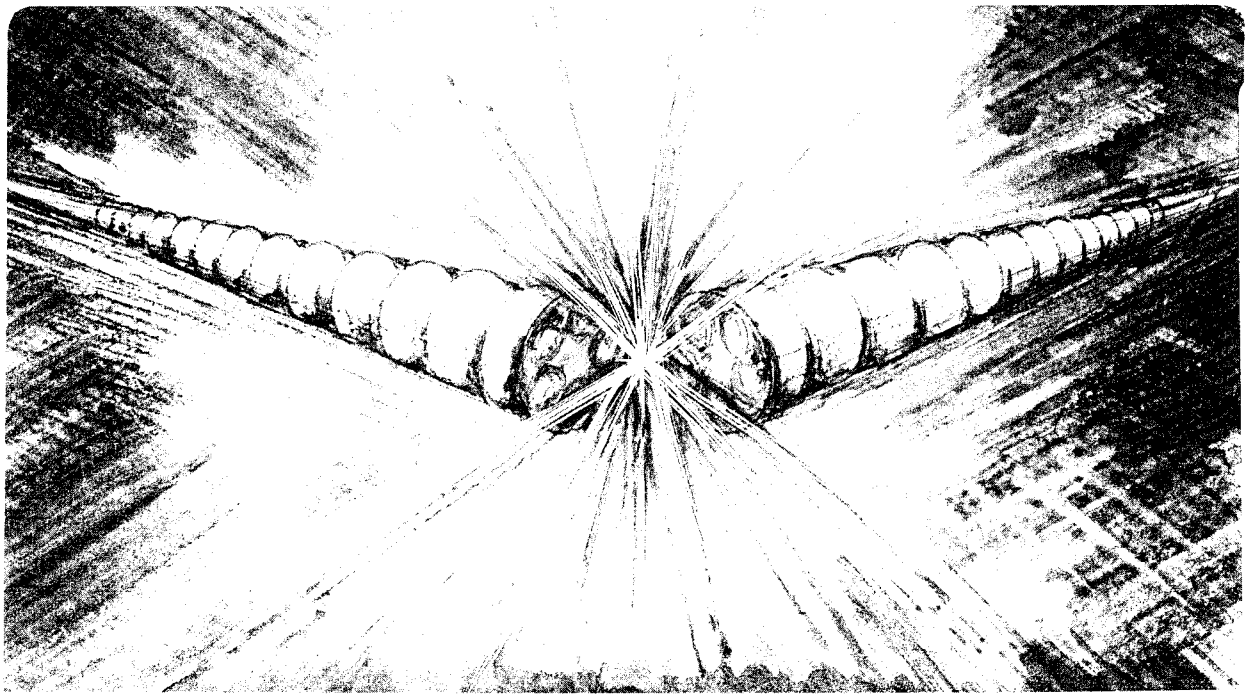

Prepared for the U.S. Department of Energy under Contract Number DE-AC03-76SF00098

LBL-30418

Standing-Wave Free-Electron Laser Two-Beam Accelerator

Andrew M. Sessler and David H. Whittum*

Lawrence Berkeley Laboratory, University of California, Berkeley, California 94720

Jonathan S. Wurtele**

Department of Physics, Massachusetts Institute of Technology, Cambridge, Massachusetts, 02139

William M. Sharp and Michael A. Makowski***

Lawrence Livermore National Laboratory, University of California, Livermore, California, 94550

February 1991

* Work at LBL was supported by the Office of Energy Research, U.S. Dept. of Energy, under Contract No DE-AC03-76SF00098.

** Work at MIT was supported by the Division of Nuclear and High Energy Physics, U.S. Dept. of Energy.

*** Work at LLNL was supported by DOE Contract No. W-7405-ENG-48.

Standing-wave free-electron laser two-beam accelerator

Andrew M. Sessler and David H. Whittum[a]

Lawrence Berkeley Laboratory, University of California, Berkeley, California 94720

Jonathan S. Wurtele

Department of Physics, Massachusetts Institute of Technology, Cambridge, Massachusetts, 02139

William M. Sharp and Michael A. Makowski

Lawrence Livermore National Laboratory, University of California, Livermore, California, 94550

Received

A free-electron laser (FEL) two-beam accelerator (TBA) is proposed, in which the FEL interaction takes place in a series of drive cavities, rather than in a waveguide. Each drive cavity is "beat-coupled" to a section of the accelerating structure. This standing-wave TBA is investigated theoretically and numerically, with analyses included of microwave extraction, growth of the FEL signal through saturation, equilibrium longitudinal beam dynamics following saturation, and sensitivity of the microwave amplitude and phase to errors in current and energy. It is found that phase errors due to current jitter are substantially reduced from previous versions of the TBA. Analytic scalings and numerical simulations are used to obtain an illustrative TBA parameter set.

1. Introduction

The next generation of linear colliders will require accelerating gradients of 100 MeV/m or more to achieve TeV energies in a machine of reasonable length [1,2]. Such a gradient corresponds to a microwave power of more than 10 J/m. A number of additional constraints [1,3] restrict the range of operating frequencies for such a linac to 10-30 GHz. In this frequency range, the free-electron laser (FEL) and the relativistic klystron (RK) have demonstrated the required power levels [4,5], and they have been proposed as microwave power sources for a TeV collider [6,7] in a configuration known as the "Two-Beam Accelerator" (TBA).

The TBA was first proposed in 1982 [8] and has been the focus of much research since that time [9,10,11]. In the TBA, a relativistic, high-current electron beam is transported through as many as one hundred FEL wiggler periods or RK cavities. This "drive" beam is alternately reaccelerated by induction cells (superconducting cavities are also being considered) and deaccelerated through its interaction with the RK or FEL microwave generation units. Microwave power is extracted and then coupled into a slow-wave structure, where it accelerates an extremely relativistic electron beam of low average current. A recent FEL/TBA conceptual design, based on the induction accelerator, is depicted in Fig. 1.

There are two important differences between the FEL and RK configurations: (1) the method of extraction of microwave power from the drive structure to the accelerating structure and (2) the short wavelength scalings. In the RK/TBA, microwave extraction is straightforward. However,

operation of the RK appears to be limited to the X-band, or lower frequencies, as indicated by experimental studies at 11.4 GHz [5]. No such wavelength limit exists for the FEL, which has been operated successfully in an over-moded waveguide at 35 GHz [4], and much higher frequencies. On the other hand, in the FEL/TBA, microwave extraction has posed a difficult problem. The original method proposed for extraction from the FEL/TBA was the "septum-coupler" [12]. Subsequent experimental work showed that a particular septum-coupling design to be limited by breakdown at low microwave power levels. It remains unclear whether this limit applies more generally to other septum-couplers. Other extraction methods have been studied and are illustrated in Fig. 2 and none of them has been found completely satisfactory.

Motivated by the need to solve the microwave extraction problem, and the advantageous scaling of the FEL through and beyond the X-band, we propose and study in this work a new TBA configuration, the standing-wave FEL/TBA. The method of extraction is "beat-coupling" as proposed by H. Henke for a recent RK/TBA design [13], and is discussed at length in Sec. 2. The conceptual layout of a single period of the new TBA is depicted in Fig. 3.

The FEL interaction in this new configuration differs from that of previous designs in an important way in that it makes use of a standing-wave cavity rather than a waveguide for the drive beam interaction region. The standing-wave FEL interaction thus takes place in the strong-slippage regime, with zero group velocity for the signal field. As a result, microwave extraction is simplified. In addition, the peak microwave power is lower and,

furthermore, need not propagate through the acceleration cells, which certainly reduces breakdown problems.

An important feature of this new configuration, is that reaccelerations are small and frequent, so that the induction cell voltage reduces approximately to a continuous axial electric field. As noted recently by Ho, Pantell and Feinstein [14], use of an axial electric field, while formally equivalent to tapering, results in a much higher efficiency. This is confirmed in our analysis of the FEL interaction, in Sec. 3. We also show that the induction cell voltage profile (as a function of time) determines the beam equilibrium (in which the beam energy is approximately constant) and stability, and represents an important, new degree of freedom in design for the standing-wave FEL.

In Sec. 4 we study the device numerically, using a one-dimensional particle simulation code. We confirm the analytic work described in Sec. 3 and study the sensitivity of output microwave amplitude and phase to jitter in the drive beam current and energy. We find that sensitivity is reduced compared to previous designs [15].

In Sec. 5, we present a formalism for studying both transverse and longitudinal multiple mode effects, as each are known to have been important in previous TBA designs [16,17,18]. Simple estimates are made to confirm the single mode model of Sec. 3.

Finally, in Sec. 6 we offer some conclusions and directions for further work.

2. Microwave extraction

At the simplest level, microwave energy transfer from the FEL cavities to the high-gradient structure may be modeled by a pair of inductively coupled resonant series RLC circuits, as shown in Fig. 4. The object of any such model is to determine the quality of the cavity coupling, as embodied in (1) the ratio, R, of the peak stored energy in cavity 2 to that in cavity 1 and (2) the phase shift, $\Delta\varphi$, in the second cavity due to deviations in the exciting voltage $V(t)$ (i.e., the drive beam) from its design specifications. We proceed to analyze R and $\Delta\varphi$.

The circuit equations for this system are

$$\begin{aligned} V(t) &= R_1 I_1 + L_1 \frac{dI_1}{dt} + \frac{1}{C_1}\int I_1\,dt + M\frac{dI_2}{dt}\,, \\ 0 &= R_2 I_2 + L_2 \frac{dI_2}{dt} + \frac{1}{C_2}\int I_2\,dt + M\frac{dI_1}{dt}\,, \end{aligned} \tag{1}$$

where R_i, L_i, and C_i (i=1,2) are the respective resistance, inductance, and capacitance of circuits 1 and 2, M is the mutual inductance between the two circuits, and $V(t)$ is a driving voltage. Two currents, I_1 and I_2 in this model, represent the microwave excitation in the two cavities. A dimensionless coupling constant, κ, is defined through M as $\kappa = M/\sqrt{L_1 L_2}$. Equation (1) can be rearranged to yield

$$\begin{aligned} \ddot{I}_1 + \nu_1 \dot{I}_1 + \omega_1^2 I_1 &= -\frac{\kappa}{\rho}\ddot{I}_2 + \frac{1}{L_1}\dot{V}_1\,, \\ \ddot{I}_2 + \nu_2 \dot{I}_2 + \omega_2^2 I_2 &= -\rho\kappa\ddot{I}_1\,, \end{aligned} \tag{2}$$

where $\nu_1 = R_1/L_1$, $\nu_2 = R_2/L_2$, $\omega_1^2 = 1/L_1C_1$, $\omega_2^2 = 1/L_2C_2$, and $\rho = \sqrt{L_1/L_2}$. Energy is transferred periodically between the cavities at the beat frequency given by $\omega_b = \kappa\omega_0/2$, where ω_0 is the unperturbed resonant frequency of the two cavities under matched ($\omega_1 = \omega_2$) conditions.

We model excitation of the drive cavity with a step pulse,

$$V(t) = \begin{cases} V_0 \cos \omega_d t, & 0 \le t \le t_p \\ 0, & \text{otherwise} \end{cases} , \tag{3}$$

where V_0 is the amplitude, ω_d is the angular frequency and t_p is the duration of the drive pulse. Note that, in general, the solution to Eq. (2) can be decomposed into symmetric and antisymmetric modes. The antisymmetric mode is the desired mode of operation, since it maximizes R. We proceed to apply Eqs. (2) and (3) to compute R and $\Delta\varphi$, due to deviations in ω_d and t_p from their design values.

We adopt dimensionless variables τ_p, the excitation pulse duration normalized to the beat time ($t_b = 2\pi/\omega_B$), given by

$$\tau_p = \frac{t_p}{t_b} = \frac{\kappa\omega_0 t_p}{4\pi} , \tag{4}$$

and $\delta\omega/\omega$, the frequency mismatch, given by

$$\frac{\delta\omega}{\omega} = \frac{\omega_1 - \omega_d}{\omega_1} . \tag{5}$$

We consider initially unexcited cavities and assume $\nu_1 = \nu_2$, $\omega_1 = \omega_2$, and $\rho = 1$. Rather than write out the somewhat cumbersome analytic solution, we will consider simple figures generated numerically.

In Fig. 5, the energy transfer efficiency, R is plotted versus τ_p for various values of $\delta\omega/\omega$, and in Fig. 6, R is plotted versus $\delta\omega/\omega$, for various values of τ_p. Evidently, $R \sim 1$ and varies only weakly with the frequency mismatch. Thus the energy in the drive cavity (cavity 1) is reliably transferred to cavity 2. In some case, $R<1$, due to dissipation ($\nu_1, \nu_2 \neq 0$), and in some cases, $R>1$, due to excitation of both symmetric and antisymmetric modes with a long pulse. Mixing of modes due to large τ_p also changes the time at which the peak current in cavity 2 occurs, increasing it from the expected value of $t_b/4$.

In Fig. 7, the phase error, $\Delta\varphi$ is plotted versus τ_p for various values of $\delta\omega/\omega$, and in Fig. 8, $\Delta\varphi$ is plotted versus $\delta\omega/\omega$, for various values of τ_p. For this example, we have selected design parameters $\delta\omega/\omega = 0$ and $\tau_P = 1 \times 10^{-2}$, and $\Delta\varphi$ is computed as the change in phase from this design case. The various wiggles present in the curves are due to terms of order ν/ω_d, $\delta\omega/\omega$, and $\tau_p\omega_b \sim \kappa$. Analytically, the phase shift is given by $\Delta\varphi \sim t_p\delta\omega/2 = (2\pi\tau_p/\kappa)(\delta\omega/\omega)$. Evidently, $\Delta\varphi$ is much more sensitive than R to $\delta\omega/\omega$ and τ_P.

From this circuit analysis, we obtain a tolerance on the allowable pulse length error and frequency mismatch of the FEL output. Of course, the utility of the TBA as a microwave source requires low jitter in phase and amplitude of the output power. This in turn requires low jitter in drive-beam current and energy, and judicious design to avoid extreme phase sensitivity to current and energy. The quantitative constraint on phase-jitter, $\Delta\varphi$ in the microwave source may be determined by computing the resulting

momentum error in the high energy beam. An average of the axial electric field in the high-gradient structure gives $\Delta P/P \sim \Delta\varphi^2/4$. In linear colliders, the allowable momentum error, $\Delta P/P$, is determined by the chromatic acceptance of the final focus, and for recent designs [19] this value ranges between 0.1% and 1%. The corresponding phase fluctuations are then $\Delta\varphi \sim 3°\text{-}10°$. To determine the corresponding constraints on beam current and energy requires a detailed analysis of the FEL interaction [15,20]. For this work we will limit ourselves to a numerical survey of the dependence (Sec. 4).

As an example, suppose that a phase shift of 5° (0.1 rad) were acceptable. From Fig. (7), we see that for $\tau_P = 1\text{x}10^{-2}$, the maximum tolerable $\delta\omega/\omega \sim 5\text{x}10^{-3}$. From Fig. (8), we see that for $\delta\omega/\omega = 1\text{x}10^{-2}$, the pulse length should lie in the interval, $1\text{x}10^{-2} < \tau_P < 3.8\text{x}10^{-2}$. We show in Sec. 4 that such tolerances may reasonably be met by typical FEL parameters.

3. Theory of the standing-wave FEL

In this section we examine the FEL interaction in the drive cavity. In Sec. 3.1 we set down the FEL equations, and in Sec. 3.2 we derive the linear growth rate for an initially unbunched beam. Finally, we consider the equilibrium propagation of a well-bunched beam in Sec. 3.3 , and examine stability against debunching. Much of this analysis, though presented previously, has not yet been published [20, 21].

2.1 Standing-wave FEL equations

We model the discrete series of drive cavities and induction cells as a continuum by averaging the axial electric field over the reacceleration period. The motion of the j^{th} electron is governed by a pair of wiggle-averaged equations for the total energy, γ_j, in units of $m_e c^2$, and the particle phase, θ_j. (The electron mass is m_e and the speed of light is c.) Betatron oscillations and mode-amplitude variations over the electron beam are neglected. The beam is assumed to couple only with a TE_{01} waveguide mode, which, by design, is usually the closest to resonance and the most strongly coupled mode. In a rectangular waveguide with height h and width w, the axial wavenumber for this mode is $k_s = (\omega_s^2/c^2 - \pi^2/h^2)^{1/2}$, where ω_s is the angular frequency of the microwave signal. For the fields, we assume an idealized planar wiggler with a vector potential

$$\vec{A}_w = \frac{m_e c^2}{e} a_w \cos\ (\ k_w z\ )\ \hat{x} \tag{6}$$

and a signal field with vector potential

$$\vec{A}_s = \frac{m_e c^2}{e} a_s \sin\left(\frac{\pi y}{h}\right) \cos\ (\ k_s z - \omega_s t + \varphi\ )\ \hat{x} \tag{7}$$

where $-e$ is the electron charge.

We assume $a_w/\gamma_j << 1$, and $a_s << a_w$. Both a_s and φ are assumed to be slowly varying compared with the fast spatial scale, $2\pi/k_s$, and the fast

temporal scale, $2\pi/\omega_s$. (The former assumption renders the equations inappropriate for modeling waveguide modes near cutoff.)

With these approximations, the wiggler-averaged particle equations are identical to those of conventional single-mode FEL theory [22],

$$\frac{d\theta_j}{dz} = k_w + k_s - \frac{\omega_s}{c} - \frac{\omega_s}{2c\gamma_j^2}\left[1 + \frac{a_w^2}{2} - 2D_x a_w\left(\hat{a_r}\cos\theta_j - \hat{a_i}\sin\theta_j\right)\right]$$
$$\frac{d\gamma_j}{dz} = -D_x\frac{\omega_s}{c}\frac{a_w}{\gamma_j}\left(\hat{a_r}\sin\theta_j + \hat{a_i}\cos\theta_j\right) - \frac{eE_z}{m_e c^2} \quad . \tag{8}$$

The coupling coefficient D_x is given by

$$D_x = \frac{1}{2}\left[J_o(\xi) - J_1(\xi)\right] \quad , \tag{9}$$

where $\xi = \omega_s a_w^2/(8ck_w\gamma_j^2) \approx (a_w/4)(1+a_w^2/2)$ and J_0 and J_1 are the zeroth and first order Bessel functions.

An equation for the complex signal amplitude, $\hat{a} \equiv \hat{a}_r + i\hat{a}_i = a_s\, exp\,(i\varphi)$, is obtained by assuming that â depends only on the distance back from the beam head, $s=V_b t - z$, where V_b~c is the average beam drift velocity. Maxwell's equations then reduce to

$$\frac{\partial\hat{a}}{\partial s} = i\eta\left\langle\frac{exp(-i\theta_j)}{\gamma_j}\right\rangle \quad , \tag{10}$$

where, the brackets denote an average over the ponderomotive bucket. This implicitly assumes an infinitesimal cavity length and ignores field coupling through the cavity irises. The coefficient η is given by

$$\eta \approx \frac{4\pi}{hw}\frac{I_b}{I_0}\frac{c}{\omega_s} D_x a_w \ , \tag{11}$$

and depends on s through the current, $I_b(s)$. The constant $I_0=m_e c^3/e\sim 17$ kA.

3.2 Linear growth

Next, we apply Eqs. (8) and (10) to an initially unbunched, monoenergetic beam and compute, to linear order in perturbed quantities, the growth of the signal field. We denote the zeroth-order detuning by

$$\Delta k = k_w + \delta k - \frac{\omega}{2\gamma_0^2 c}\left(1+\frac{a_w^2}{2}\right) \ , \tag{12}$$

where $mc^2\gamma_0$ is the initial beam energy, $\delta k = k_s - \omega_s/c$. Defining $\tilde{a}(s,z)=\hat{a}(s,z)exp(i\Delta kz)$, a linearized treatment analogous to that of Bonifacio *et al* [23], reveals that

$$\frac{\partial^3 \tilde{a}}{\partial z^2 \partial s} = i\mu\tilde{a} \ , \tag{13}$$

where

$$\mu = \frac{\omega a_w \eta}{\gamma_o^3 c} (k_w + \delta k - \Delta k) \ . \tag{14}$$

For μ independent of s (constant current), we find

$$\tilde{a}(s,z) = a_0 \sum_{n=0}^{\infty} \frac{(i\mu s z^2)^n}{n!(2n)!} \ , \tag{15}$$

where $\tilde{a}(z,s=0)=a_0$. Asymptotically, Eq. (15) takes the form

$$\tilde{a}(s,z) \approx a_0 (2^4 3^3 \pi^3 \mu s z^2)^{-1/6} exp\left\{ -i\frac{\pi}{12} + (1+i\sqrt{3})\left(\frac{3^3}{2^5}\mu s z^2\right)^{1/3} \right\} \tag{16}$$

This result bears a strong resemblance to the asymptotic growth of the beam break-up instability [24,16], as would be expected from the cumulative character of the standing-wave FEL instability. From Eq. (16), bunching at fixed s proceeds as $exp(z/L_g)^{2/3}$, where

$$L_g = \frac{2^{5/2}}{3^{3/2}} \frac{1}{\sqrt{\mu s}} \ . \tag{17}$$

At fixed z, the microwave power varies as $exp(\Gamma s)^{1/3}$, where

$$\Gamma = \frac{3^3}{2^2} \mu z^2 \ . \tag{18}$$

In practical units, taking zero detuning and small waveguide correction, δk, as an example, the growth length is $L_g/\lambda_w \sim 0.1(hwI_0/L_p\lambda_w I)^{1/2}$, where L_p is the pulse length. This growth length can be quite short, making amplification readily amenable to measurement in a "proof-of-principle" experiment. However, many-particle simulations (such as that shown in Fig. 9, and discussed below) reveal that the beam does not evolve to an equilibrium, i.e., a z-independent, well-bunched state. We conclude that to reach the desired z-independent equilibrium, appropriate for a reliable microwave power source, some form of pre-bunching is required, as we discuss next.

3.3 Equilibrium of a well-bunched beam

For a well-bunched beam, we may model each bunch with a single particle. We adopt $\delta\gamma = \gamma - \gamma_r$ and θ as dynamical variables and linearize Eq. (8) to find,

$$\frac{d\theta}{dz} \approx 2(k_w + \delta k)\frac{\delta\gamma}{\gamma_r} ,$$
$$\frac{d\delta\gamma}{dz} \approx -D_x\frac{\omega_s}{c}\frac{a_w}{\gamma_r}\left(\hat{d}_r \sin\theta + \hat{d}_i \cos\theta\right) - \frac{eE_z}{m_e c^2} , \qquad (19)$$

where γ_r, the resonant energy, corresponds to $\Delta k=0$ in Eq. (12). Looking for a z-independent equilibrium, characterized by some $\theta_0(s)$, we set $\delta\gamma=0$ in Eq. (19) to find the E_z required for equilibrium:

$$\varepsilon = -\frac{eE_z}{m_e c^2}$$
$$= D_x \frac{\omega_s}{c}\frac{a_w}{\gamma_r}(\hat{a}_r \sin\theta_0 + \hat{a}_i \cos\theta_0)$$
$$= D_x \frac{\omega_s}{c}\frac{a_w}{\gamma_r} a \sin\psi_0 \qquad (20)$$

where $\psi_0=\theta_0+\varphi$ is the equilibrium ponderomotive phase. The s-variation of ε corresponds to the induction cell voltage profile, and is intimately connected with the beam equilibrium as represented by θ_0. The components of $\hat{a}$ in Eq. (10) are obtained with an integration

$$\hat{a}(s) = \hat{a}(0) + \frac{i}{\gamma_r}\int_0^s ds'\eta(s')\exp[-i\theta_0(s')] \qquad (21)$$

As in the conventional FEL [25] or the RF linac [26], the axial motion of a test particle in the fields given by Eqs. (20) and (21) are described by the Hamiltonian of a driven nonlinear pendulum. The size of the corresponding ponderomotive potential or "bucket" determines the longitudinal acceptance. The bucket height, $\Delta\gamma$, and width, $\Delta\theta$, are in turn determined by the equilibrium ponderomotive phase $\psi_0=\theta_0+\varphi$ and the wave amplitude a, according to the well-known results,

$$\Delta\theta = \pi - 2\psi_0,$$
$$\Delta\gamma = (\Xi a)^{1/2}\left(\cos\psi_0 + \left[\psi_0 - \frac{\pi}{2}\right]\sin\psi_0\right)^{1/2}, \qquad (22)$$

where the constant

$$\Xi = 2D_x a_w \frac{\omega_s/c}{k_w + \delta k}. \tag{23}$$

Some insight into the variation in s of the bucket size can be obtained by examining the variation in $2\pi/k_B$, the bounce period for small oscillations in θ. From Eq. (19),

$$k_B^2 = \kappa^2 a \cos \psi_0, \tag{24}$$

where

$$\kappa^2 = 2 (k_w + \delta k) D_x \frac{\omega_s}{c} \frac{a_w}{\gamma_r}. \tag{25}$$

From Eq. (21) we find

$$\frac{\partial}{\partial s} k_B^2 = - \kappa^2 a \sin \psi_0 \frac{\partial}{\partial s} \theta_0, \tag{26}$$

(valid for arbitrary θ_0, η). Thus longitudinal focussing is non-increasing in s, unless detuning is positive (so the variation of θ_0 in s is negative). (Implicitly we assume $a \sin \psi_0 > 0$ corresponding to a positive reacceleration field in Eq. (20).)

As a practical special case, we consider a beam which is prebunched at a frequency $\omega_S + \Delta\omega$, so that

$$\theta_0(s) = \alpha - \frac{\Delta\omega}{V_b} s = \alpha + \beta s \quad , \tag{27}$$

where α and β are constants. In general, for a specified current profile, it is often possible to calculate all quantities of interest analytically. Qualitative insight is obtained by considering the case of constant current (η constant), with some nonzero input power ($a_0 \neq 0$). From Eq. (20), the reacceleration field required to maintain this equilibrium is

$$\varepsilon = D_x \frac{\omega_s}{c} \frac{a_w}{\gamma_r} \left[\hat{a_r}(0) \sin(\alpha + \beta s) + \hat{a_i}(0) \cos(\alpha + \beta s) + \frac{\eta}{\beta\gamma_r} \sin(\beta s) \right] , \tag{28}$$

and the components of $\hat{a}$ are given by

$$\begin{aligned} \hat{a_r}(s) &= \hat{a_r}(0) + \frac{\eta}{\beta\gamma_r} [\cos(\alpha) - \cos(\alpha + \beta s)] \quad , \\ \hat{a_i}(s) &= \hat{a_i}(0) - \frac{\eta}{\beta\gamma_r} [\sin(\alpha) - \sin(\alpha + \beta s)] \quad . \end{aligned} \tag{29}$$

The growth in microwave power is given by

$$\begin{aligned} a(s)^2 - a(0)^2 = \\ 2\frac{\eta a(0)}{\beta\gamma} [\cos(\alpha + \varphi_0) - \cos(\alpha + \varphi_0 + \beta s)] + \left(\frac{2\eta}{\beta\gamma}\right)^2 \sin^2\left(\frac{\beta s}{2}\right) . \end{aligned} \tag{30}$$

A straightforward but tedious calculation shows that the minimum bucket width and height are given by [21]

$$\Delta\theta \approx 3\left(-\frac{\beta\gamma_r}{\eta}a_0\right)^{1/2},$$
$$\Delta\gamma \approx 3\left(-\frac{\beta\gamma_r \Xi}{\eta}\right)^{1/2} a_0, \qquad (31)$$

where again $\delta k = k_S - \omega_S/c$. This result shows that the bucket vanishes when β is zero or positive and that the longitudinal acceptance $\Delta\theta\,\Delta\gamma$ increases with a larger initial signal and larger $-\beta/\eta$.

The energy deposited per unit length is

$$W_{out} \approx \frac{1}{c} Z_o I^2 \left(2 D_x \frac{a_w}{\gamma_r}\right)^2 \frac{L_p^2}{hw}\left(\frac{\sin(\beta L_p/2)}{\beta L_p/2}\right)^2, \qquad (32)$$

where Z_0~377 Ω, L_p is the pulse length and $O(a_0)$ terms are neglected.

To check these results and to gain more insight into the particle motion, we resort to many-particle simulations. We shall see that Eq. (31) underestimates the acceptance for distributions with spreads in θ and γ because the required reacceleration field in such cases is somewhat lower than that needed for the single-particle case.

4. Numerical studies

4.1 Input parameters

The operating frequency ω_s and the final energy per unit length W_{out} left in the cavities are determined, in practice, by the TBA requirements.

With these quantities given, the specification of the waveguide dimensions, h and w, the wiggler wavelength, $\lambda_w = 2\pi/k_w$, and the wiggler strength, a_w, fixes the principal beam parameters. The beam energy is determined by the resonance condition, and the total beam charge, given by $I_b L_b/V_b$ is set by the output microwave energy, W_{out}. Since the initial spreads in θ and γ are determined by both the intrinsic emittance from the accelerator and the additional emittance introduced by prebunching, these values are not considered free parameters.

Two remaining beam quantities, the beam current envelope $I_b(s)/\max I_b$ and the prebunching factor β, can be chosen by practical considerations. Since the acceptance is found to be proportional to I_b^{-1}, it is preferable for the current to be low near the beam head, where the bucket is smallest. It is also found from the single-particle equations that a current which increases linearly or faster in s leads to a reacceleration field E_z that is monotonically increasing for $s \leq L_b$. This field form is easier to generate for a short pulse. For these reasons, we typically study beams with a uniform current ramp. The prebunching factor is chosen by considering the β-dependences of various beam quantities obtained from the single-particle solution. We find that the required beam charge and the longitudinal acceptance increase with βL_b, while the maximum reacceleration field decreases. Since the longitudinal beam emittance is difficult to decrease in induction accelerators, we choose $\beta L_b = \pi$. .

The nominal parameters used in the simulations here are listed in Table 1, and we typically run the simulation with a wiggler length $L_w = 40$ m.

These values are appropriate for a generic TBA, and little effort has been made to optimize the waveguide size or the wiggler strength and wavelength.

4.2 Initialization

The simulation initialization parallels the single-particle equilibrium solution. A distribution with prescribed spreads $\Delta\theta_0$ and $\Delta\gamma_0$ in θ_j and γ_j, is loaded so that $\langle\theta_j\rangle = \alpha + \beta s$ and $\langle\gamma_j\rangle = \gamma_r$. Simulation particles are randomly distributed within this phase-space rectangle, and different random positions are chosen for each beam slice. Although this distribution is somewhat idealized, it allows for the longitudinal acceptance to be tested systematically. For the small spreads in θ_j and γ_j treated here, 200 simulation particles are adequate to give tolerably low statistical noise.

The normalized reacceleration field defined in Eq. (19) required to keep $\langle\gamma_j\rangle$ constant is given by

$$\varepsilon = D_x \frac{\omega_s}{c} a_w \left(\hat{a_r} \left\langle \frac{\sin\theta_j}{\gamma_j} \right\rangle + \hat{a_i} \left\langle \frac{\cos\theta_j}{\gamma_j} \right\rangle \right) . \tag{33}$$

This field could be recalculated at each z and s value, but such an algorithm introduces a high-frequency noise component in ε that increases exponentially with z. A more practical approach is to calculate $\varepsilon(s)$ at $z = 0$ and to use it at all subsequent z positions. With this second technique, the calculated ε is noise free and reduces to Eq. (19) in the limit that $\Delta\theta_0$ and $\Delta\gamma_0$ are zero.

We determine the initial signal level, $|\hat{a}(0)|$, by assuming an input microwave power per unit length, P_{in}, and then balancing this with cavity wall losses which are specified by using an assumed cavity Q.

4.3 Numerical simulation results

The output microwave energy W_{out} and phase ϕ for a beam with the nominal parameters and a linearly increasing I_b are shown in Fig. 10. The spreads $\Delta\theta_0 = 0.1$ and $\Delta\gamma_0 = 0.01$ used here are small enough that the distribution remains trapped and the output signal is reasonably insensitive to beam and field errors. The principal z-dependence in Fig. 10 is the initial ripple in W_{out} due to synchrotron motion, which corresponds to a 2% fluctuation in the average electron energy. This ripple does not fully damp in the 40 m wiggler because the deeply trapped distribution randomizes very slowly. There is also a low amplitude ripple in the wave phase ϕ that results from fluctuations in $\langle \cos(\theta_j + \phi)/\gamma_j \rangle$, due again to synchrotron motion. The wavelength in z of this phase ripple corresponds to the synchrotron wavelength in the initial field because $\partial\phi/\partial s$ from Eq. (10) is proportional to a^{-1}, which is largest at small s.

For the standard case, the greatest sensitivity to parameter errors is found for fluctuations in the initial energy. When the reacceleration field is calculated for a beam at the resonant energy and the simulation is then run with an energy that is 1% higher, W_{out} is nearly unaffected, but ϕ, shown in Fig. 11(a), develops a ripple in z of about $\pi/2$ radians. As in the case with no detuning, the ripple wavelength corresponds to the synchrotron wavelength

in the initial field, but the amplitude is significantly larger because the distribution centroid is well away from the bucket center and executes large orbits in θ. This phase ripple can be reduced by choosing a larger a_0, which makes the initial bucket larger, or by decreasing a_w while adjusting λ_w or the waveguide dimensions to maintain constant γ_r.

As discussed in Sec. 2 the tolerance on $\Delta\phi$ fluctuations will likely be in the range 0.06 to 0.2 radians. While these values are somewhat less than shown in Fig. 11 (a), the 1% energy error used in that case is higher than present experimental values achieved in induction linacs [27]. Aside from improvements in induction-linac energy regulation, there are several other techniques that might reduce the magnitude of FEL phase fluctuations, such as use of an energy selector before the FEL or the introduction of correlations between the energy error and the prebunching parameters α and β.

Phase ripple is also introduced by variations in the average energy with s, which can develop in an accelerator due to beam loading. As an illustration, Fig. 11b shows ϕ for a beam with an energy equal to γ_r at the beam head and dropping gradually by 4% toward the beam tail. The phase ripple for this case is similar to the equilibrium (constant energy) case in Fig. 10 because the beam distribution remains near the bucket center while the signal amplitude is small.

In contrast to the sensitivity to detuning, a 2% error in I_b has a negligible effect on both W_{out} and ϕ. A change of 2% in the magnitude of ε likewise has little effect on both the output energy and phase for the parameters studied here, but introducing a 0.1 ns time lag in the reacceleration field again causes a long wavelength ripple of about $\pi/2$ in ϕ, as

shown in Fig. 12a. This ripple results from a beam energy loss during the initial period (<0.1 ns) when $\varepsilon = 0$, which causes the beam, in effect, to be detuned. The assumption of a constant time lag, of course, corresponds to a worst case. A more realistic jitter model lets the ε timing error vary randomly over a scale length in z equal to λ_w. The wave phase for such a case, with a root mean-square jitter of 0.1 ns, is plotted in Fig. 12b. It shows a phase ripple of about $\pi/8$.

Studies with a constant-current beam show that the final wave phase is as stable as that of a beam with a linear current ramp, but, in addition, there is a 10% ripple in W_{out} that persists throughout the FEL. A beam with constant I_b also begins to lose particles when errors in energy or current exceed about 1.5%, indicating the reduced acceptance for this current envelope.

5. Multiple mode effects

In this section, we describe the excitation of parasitic modes by a well-bunched beam, making use of a wakefield analysis appropriately modified to include the effect of the off-axis excursions of the wiggler orbit.

We start from Maxwell's equations for the vector potential in terms of the beam current density,

$$\left(\nabla_\perp^2 + \frac{\partial^2}{\partial z^2} - \frac{1}{c^2}\frac{\partial^2}{\partial t^2}\right)\vec{A} = -\frac{4\pi}{c}\vec{J}, \tag{34}$$

and then decompose the vector potential into a sum over the modes of the cavity,

$$\vec{A} = \frac{mc^2}{e}\sum_{\alpha} q_{\alpha}(t)\,\vec{a}_{\alpha}(\vec{r}\,) \quad , \tag{35}$$

where α is the mode index, q_α is the mode amplitude and $\vec{a}_\alpha$ gives the spatial dependence of the mode. The normalization

$$\int_V d^3 r'\,\vec{a}_{\alpha}(\vec{r}\,) \bullet \vec{a}^{*}_{\alpha}(\vec{r}\,) = V \tag{36}$$

is assumed, with V the cavity volume. Substituting Eq. (35) into (34) results in an equation for the amplitude, q_α, of the mode α,

$$\left(\frac{\partial^2}{\partial t^2} + \frac{\omega_\alpha}{Q_\alpha}\frac{\partial}{\partial t} + \omega_\alpha^2\right) q_{\alpha}(t) = \frac{4\pi e}{mc}\frac{1}{V}\int_V d^3 r'\,\vec{J}\,(\vec{r}\,',t) \bullet \vec{a}^{*}_{\alpha}(\vec{r}\,') \quad , \tag{37}$$

where we model dissipation with a phenomenological quality factor, Q_α. The resonant angular frequency, ω_α, of the mode α is shifted to $\Omega_\alpha = (\omega_\alpha^2 - \nu_\alpha^2)^{1/2}$ due to losses where $\nu_\alpha = \omega_\alpha / 2\,Q_\alpha$.

Next, we write the current density as

$$\vec{J}\,(\vec{r}_\perp, z, s) = I_b(s)\,\delta^2(\vec{r}_\perp - \vec{r}_w(z))\,\frac{\vec{v}\,(z)}{v_z} \quad , \tag{38}$$

with

$$\vec{v}\,(z) = v_z\hat{z} + \vec{v}_w(z) \quad , \tag{39}$$

where r_w and v_w are, respectively, the trajectory and velocity in the transverse plane due to the wiggler field, and are assumed to depend only on z. The variable $s=v_z t-z$, and we assume $I_b(s)=0$ for $s<0$. Variation of v_z in z is neglected. For brevity we will denote $\vec{a}_\alpha^*(\vec{r}_w(z),z)$ by $\vec{a}_\alpha^*(z)$.

The solution for q_α is then given up to quadrature by

$$q_\alpha(t)=\frac{4\pi e}{mc}\frac{1}{V}\int_0^t dt'\, G_\alpha(t-t')\int_{-L/2}^{+L/2} dz \frac{\vec{v}(z)}{v_z}\bullet\vec{a}_\alpha^*(z)I_b(v_z t'-z) \tag{40}$$

where the cavity length is L, and the Green's function for the mode is given by

$$G_\alpha(t)=\frac{\sin(\Omega_\alpha t)}{\Omega_\alpha}\exp(-\nu_\alpha t/2) \tag{41}$$

The electric field takes the form

$$\begin{aligned}\vec{E}(\vec{r},t)=-\frac{4\pi}{V}\sum_\alpha \vec{a}_\alpha(\vec{r})\int_0^t dt'\frac{\partial G_\alpha}{\partial t}(t-t')\rightarrow \\ \rightarrow\int_{-L/2}^{+L/2} dz'\frac{\vec{v}(z')}{v_z}\bullet\vec{a}_\alpha^*(z')I_b(v_z t'-z')\end{aligned} \tag{42}$$

To determine the energy deposited by the beam, we apply Eq. (42) to compute the voltage drop experienced by an electron at s in traversing the cavity,

$$V(s) = \int_{-L/2}^{+L/2} dz \frac{\vec{v}(z)}{v_z} \bullet \vec{E}\left(\vec{r}_w(z), \frac{s+z}{v_z}\right)$$
$$= \int_0^s ds' \, I_b(s') \, W(s-s') \quad , \tag{43}$$

where the wake potential may be expressed as sum over the wakes from each mode,

$$W(s) = \sum_\alpha W_\alpha(s) \quad . \tag{44}$$

These wakes W_α are longitudinal wakefields in the sense that they from the loss of beam energy and are nonzero on the design orbit. The dominant contribution to W is from the FEL term, $\vec{v}_w \cdot \vec{a}_\alpha$, with α the TE_{01} mode in our example. The wakes are most simply expressed in terms of their Fourier transform, Z_α, the impedance of the magnetized cavity, due to mode α,

$$Z_\alpha(\omega) = \frac{4\pi}{V} i\omega \tilde{G}_\alpha(\omega) \left| \int_{-L/2}^{+L/2} dz \frac{\vec{v}(z)}{v_z} \bullet \vec{a}_\alpha(z) \exp\left(-\frac{i\omega z}{v_z}\right) \right|^2 \quad , \tag{45}$$

where the tilde denotes the Fourier transform. From Eq. (41), this may be expressed as

$$Z_\alpha(\omega) = \frac{i\omega\omega_\alpha}{\omega_\alpha^2 - \omega^2 - i\frac{\omega\omega_\alpha}{Q_\alpha}} (R/Q)_\alpha \quad , \tag{46}$$

where the "surge impedance" is

$$(R/Q)_{\alpha} = \frac{4\pi}{V\omega_{\alpha}} \left| \int_{-L/2}^{+L/2} dz \frac{\vec{v}(z)}{v_z} \bullet \vec{a}_{\alpha}(z) \exp\left(-\frac{i\omega z}{v_z}\right) \right|^2 . \tag{47}$$

As for more conventional, unmagnetized cavities, the "R upon Q" provides a simple estimate of the power coupled into the mode α. Applying Eq. (49) we may compare the coupling to the design mode, with that of competing, parasitic modes in the drive cavity.

We find for the design TE_{01p} mode,

$$R/Q = \frac{Z_0}{8\pi} \frac{\lambda L}{hw} \left(\frac{a_w}{\gamma}\right)^2 , \tag{48}$$

where Z_0=377 Ω. Not surprisingly, the coupling may be adjusted through a_w.

For a $TM_{m,1,p'}$ mode we find

$$R/Q = \frac{Z_0}{4\pi} \frac{\lambda L}{hw} \left\{ \frac{k_x^2 + k_y^2}{k_x^2 + k_y^2 + k_z^2} \right\} \left(\frac{\sin\theta}{\theta}\right)^2 , \tag{49}$$

where $\theta = (p\pi \pm \omega L/v_z)/2$ is the transit angle. With a large transit angle, this can be made quite small. (On the other hand, for the design mode, the transit angle is always small because it is measured with respect to the fast-wave resonance.)

For a nearby $TE_{m1p'}$ modes, we find

$$R/Q = \frac{Z_0}{4\pi}\frac{\lambda L}{hw}\left(\frac{a_w}{\gamma_r}\right)^2\left\{\frac{k_y^2}{k_x^2+k_y^2}\right\}\left(\frac{\sin\theta}{\theta}\right)^2, \qquad (50)$$

where $\theta = (\omega L/v_z - p\pi - k_w L)/2$.

It should be emphasized that the estimates, Eqs. (48)-(50), rely on the fields of a closed pillbox, and neglect fringe field effects at the beam ports, which, in principle, can be important in determining the actual impedances. In addition, the detailed physics of longitudinal and transverse mode locking merits further study.

6. Discussion

We have presented the concept of a standing-wave free-electron laser Two-Beam Accelerator, in which the drive beam, as it traverses the wiggler, propagates through a series of overmoded cavities. The drive beam is reaccelerated frequently so that its energy remains roughly constant. Microwaves are extracted, by means of a side-coupler, to a single-mode waveguide which is, in turn, coupled to an accelerating cavity.

The standing-wave TBA has some substantial advantages over previous configurations: (1)the microwave power does not propagate through the induction gaps; (2)microwave extraction is straightforward; (2) the phase error due to current jitter has been substantially reduced; and (3) peak power levels are relatively low.

A number of problems not studied here deserve further consideration. Our idealized model of the FEL interaction has replaced the series of discrete

drive-cavities and induction cells with a continuum. A more realistic model consisting of a series of short microwave FEL oscillators, separated by induction cells and allowing for coupling between oscillators, remains to be developed. The effect of multiple modes (including beam break-up modes) and sidebands remain to be studied in detail. Orbit matching and the trade-offs between increased transverse acceptance of the drive-beamline and coupling between the FEL cavities also remain to be studied. Should a widening of the beam ports be desirable, our theory must then be modified to include a small, but non-zero, group velocity.

It is clear that much work must be done to validate the standing-wave TBA. However, the merits revealed by this study appear to justify the effort. Ultimately, the basis for choosing between an RK and an FEL version of the TBA will be determined by capital and operating cost, as well as by the ease and reliability of operation. At low frequencies, the RK is "conventional" and therefore preferable. At high frequencies, the FEL is *necessary*. The difficulty is that the transition from "low" to "high" frequencies is likely to be between 10 and 20 GHz, i.e., just in the range where one would likely operate a TBA.

Acknowledgements

We appreciate numerous helpful comments by Xiao-Tong Yu on the impedance description of multiple mode effects, and wish to note related work on this subject [28].

Work at LBL was supported by the Office of Energy Research, U.S. Dept. of Energy, under Contract No DE-AC03-76SF00098. Work at MIT was

supported by the Division of Nuclear and High Energy Physics, U.S. Dept. of Energy. Work at LLNL was supported by DOE Contract No. W-7405-ENG-48. Work in Japan at the *LC '90* conference was supported by the National Laboratory for High Energy Physics (KEK).

References

(a) Present address: Accelerator Department, National Laboratory for High Energy Physics (KEK), 1-1 Oho, Tsukuba, Ibaraki, 305, Japan.

[1] R. B. Palmer, CERN Report No. 87-11, ECFA 87/110 (CERN, Geneva, 1987) pp. 80-120.

[2] The present state of the art for rf linacs is about 20 MeV/m, at the Stanford Linear Collider. J. T. Seeman and J. C. Sheppard, Ref. 1, pp. 122-133.

[3] P.B. Wilson, *Laser Acceleration of Particles*, edited by Chan Joshi and Thomas Katsouleas, AIP Conf. Proc. **130**, 560-597 (1985) .

[4] T. J. Orzechowski, *et al.*, Phys. Rev. Lett. **54**, 889 (1985).

[5] M. A. Allen, *et al.*, Phys. Rev. Lett **63**, 2472 (1989).

[6] A. M. Sessler, E. Sternbach, J. S. Wurtele, Nucl. Instrum. Methods **B40/41**, 1064 (1989).

[7] A. M. Sessler and S. S. Yu, Phys. Rev. Lett. **58**, 2439 (1987).

[8] A. M. Sessler, *Proceedings of the Workshop on the Laser Acceleration of Particles,* C. Joshi and T. Katsouleas, eds., AIP Conf. Proc. **91**, 154 (1982).

[9] D. B. Hopkins, A. M. Sessler, J.S. Wurtele, Nucl. Instrum. Methods **228**, 15 (1984).

[10] A. M. Sessler and D. B. Hopkins, *Proceedings of the 1986 Linear Accelerator Conference*, June 2-6, 1986, 385 (SLAC, 1986).

[11] D. B. Hopkins, K. Halbach, E. H. Hoyer, A. M. Sessler, and E. J. Sternbach, *Advanced Accelerator Concepts*, edited by Chan Joshi, AIP Conf. Proc. **193**, 141-151 (1989).

[12] D. B. Hopkins, *et al., Proceedings of the 1987 IEEE Particle Accelerator Conference,* edited by Eric R. Lindstrom and Louise S. Taylor, 80-82 (1987).

[13] H. Henke, "An Energy Recuperation Scheme for a Two-Beam Accelerator", CERN Internal Report CERN-LEP-RF/8-55 (unpublished, 1988).

[14] A. H. Ho, R. H. Pantell, and J. Feinstein, *Proceedings of the 11th International Free-Electron Laser Conference,* Nucl. Instrum. Methods A**296**, 631 (1990).

[15] A. M. Sessler, D. H. Whittum and J. S. Wurtele, *Proceedings of the XIV International Conference on High Energy Accelerators,* Particle Accelerators **31**, 69 (1990).

[16] D. H. Whittum, G A. Travish, A. M. Sessler, J. F. DeFord and G. D. Craig, *Proceedings of the 1989 IEEE Particle Accelerator Conference,* edited by Floyd Bennet and Joyce Kopta, 1190 (1989).

[17] D. H. Whittum, A. M. Sessler, G. D. Craig, J. F. DeFord and D. U. L. Yu, *Advanced Accelerator Concepts,* Chan Joshi, editor, AIP Conf. Proc. **193**, 433 (1989).

[18] D. H. Whittum, A. M. Sessler, and V. K. Neil, Phys. Rev. A **43**, 294 (1991).

[19] K. Oide, *Proceedings of the 1989 IEEE Particle Accelerator Conference,* edited by Floyd Bennet and Joyce Kopta, 1319 (1989).

[20] W. M. Sharp, G. Rangarajan, A. M. Sessler, and J. S. Wurtele, *Proceedings of the International Society for Optical Engineering* (SPIE), Jan 21-24, 1991 (to be published).

[21] W. M. Sharp, A. M. Sessler, D. H. Whittum, and J. S. Wurtele, LINAC 90, Sept. 10-14, 1990, Los Alamos National Laboratory (to be published).

[22] T.J. Orzechowski, *et al.*, IEEE J. of Quantum Electronics, **QE-21**, 831 (1985).

[23] R. Bonifacio, C. Pellegrini, and L.M. Narducci, Opt. Commun. **50**, 373 (1984).

[24] Y.Y. Lau, Phys. Rev. Lett. **63**, 1141 (1989).

[25] N. M. Kroll, P. L. Morton and M. N. Rosenbluth, IEEE J. Quant. Elec. **QE-17**, 1436 (1981).

[26] Stanley Humphries, *Principles of Charged Particle Acceleration* (John Wiley & Sons, New York, 1986).

[27] S. Sampayan, G. Caporaso, Y. J. Chen, P. Decker, and W. Turner, Lawrence Livermore National Laboratory Report UCRL-JC-105043, LINAC 90, Sept. 10-14, 1990, Los Alamos National Laboratory (to be published).

[28] X. T. Yu, J. S. Wurtele, and D. H. Whittum, "Impedance formalism for an arbitrary cumulative instability" (unpublished).

FIG. 1. Conceptual schematic for a Two-Beam Accelerator (TBA).

FIG. 2. Schematic of various microwave extraction schemes which were considered in earlier versions of the TBA.

FIG. 3. Conceptual layout of one section of a standing-wave TBA. Depicted are the induction cell for reacceleration, the wiggler, the drive cavity, and the accelerating cavity .

FIG. 4. The equivalent circuit used for modeling the microwave coupling between the drive cavity and the accelerating cavity, as described by Eq. (1).

FIG. 5. Ratio, R, of the peak excitation in cavity 2 to that in cavity 1 as a function of normalized pulse length for various detunings of the $\delta\omega/\omega$ of the drive voltage.

FIG. 6. Ratio, R, of the peak excitation in cavity 2 to that in cavity 1 as a function of detuning $\delta\omega/\omega$ for various values of the normalized pulse length.

FIG. 7. Phase shift, $\Delta\varphi$, of the microwave signal in the accelerating cavity (cavity 2) due to deviation in the drive frequency or pulse length from their design values (which are $\delta\omega/\omega = 0$, and $\tau_p = 0.01$ for this example). Depicted is the phase error for various detunings as a function of normalized pulse length.

FIG. 8. Phase error, $\Delta\varphi$, as in Fig. 7, depicted for various normalized pulse lengths as a function of the frequency detuning.

FIG. 9. Phase space of a slice of an initially unbunched beam at **(a)** $z = 0$, **(b)** $z = L_w/3$, **(c)** $z = 2L_w/3$, and **(d)** $z = L_w$ in a wiggler with $L_w = 10$ m. The bucket boundaries are indicated by solid lines.

FIG. 10. Output energy per unit length W_{out} and microwave phase ϕ as functions of the interaction length z/L_w for the parameters of Table 1.

FIG. 11. Microwave phase ϕ as a function of z/L_w for a beam with **(a)** a constant energy 1% above γ_r and **(b)** an energy that is initially equal to γ_r and then decreases by 4% toward the tail of the pulse.

FIG. 12. Microwave phase ϕ as a function of z/L_w for a beam with **(a)** a 0.1 ns lag in the reacceleration field and **(b)** a reacceleration field with an rms timing jitter of 0.1 ns.

Table 1. Parameters for a standing-wave TBA, powering a 500 GeV x 500 GeV linear electron-positron collider.

Drive Beam	Drive Structure	High-Energy Beam
I_{peak} = 2.17 kA	λ_w = 25 cm	G = 100 MeV/m
E = 13.8 MeV (γ_r = 27.6)	a_w = 8.86	L = 3.6 km
L_b = 180 cm (τ_b = 6 nsec)	h x w = 3 cm x 10 cm	$N = 2 \times 10^{10}$
$\Delta\Theta$ = (0.1) 2π	f = 17.1 GHz	n = 10
$\Delta\gamma$ = (0.01) γ_r	W_{out} = 10 J/m	f_{rep} = 360 Hz

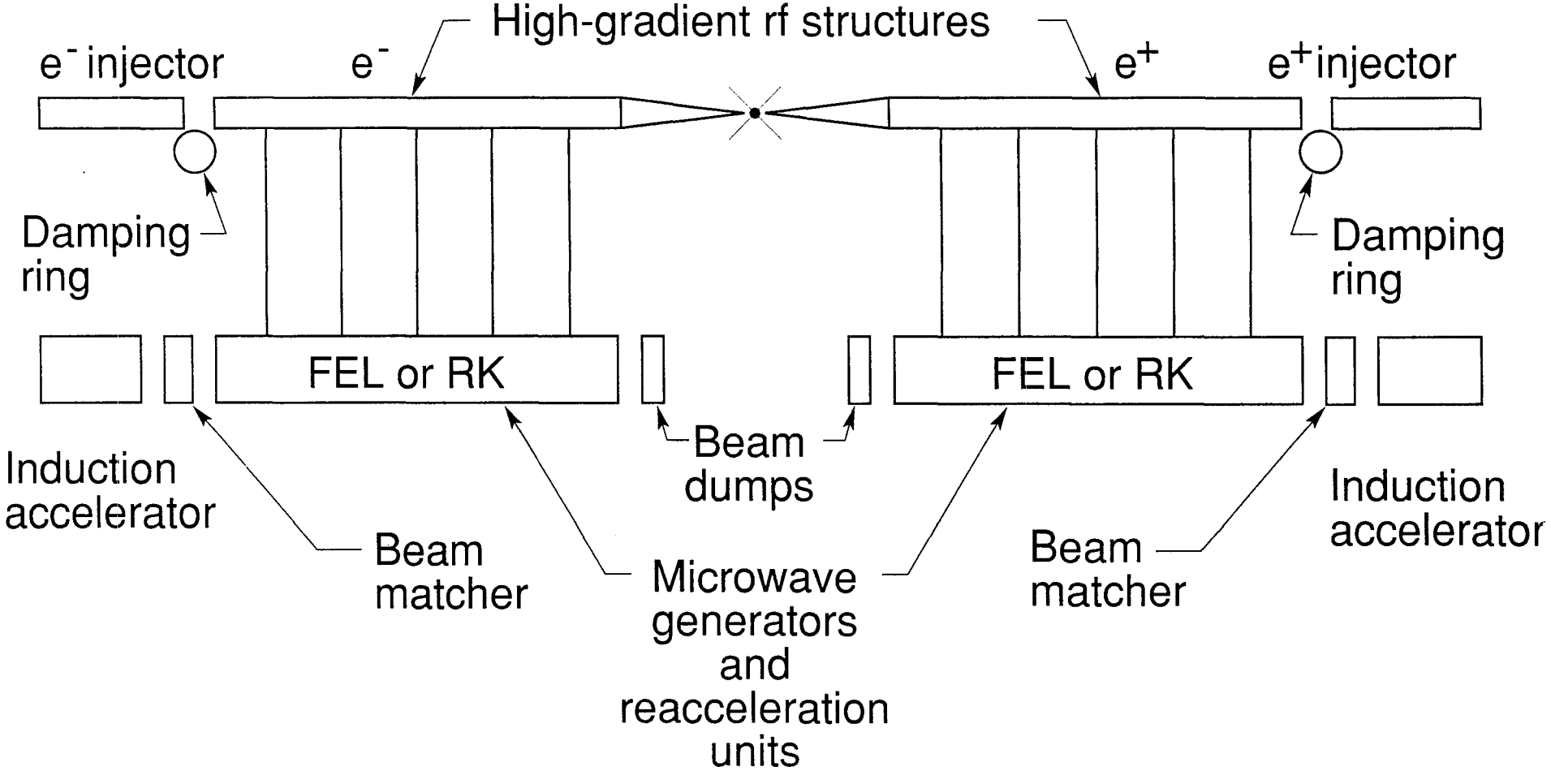

XBL 9010-5571

Fig. 1

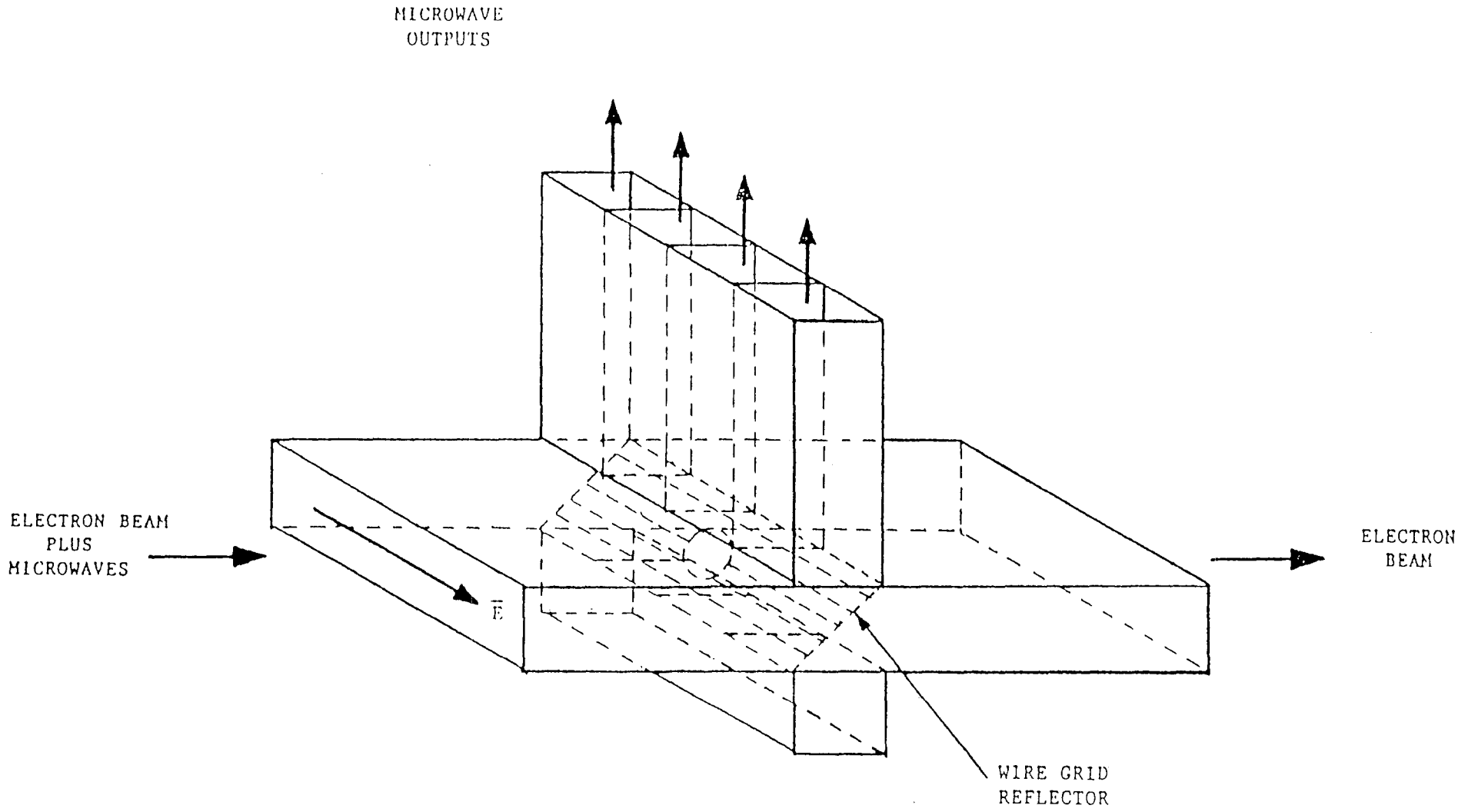
MICROWAVE
OUTPUTS
ELECTRON BEAM
PLUS
MICROWAVES
$\bar{E}$
ELECTRON
BEAM
WIRE GRID
REFLECTOR

Fig. 2a

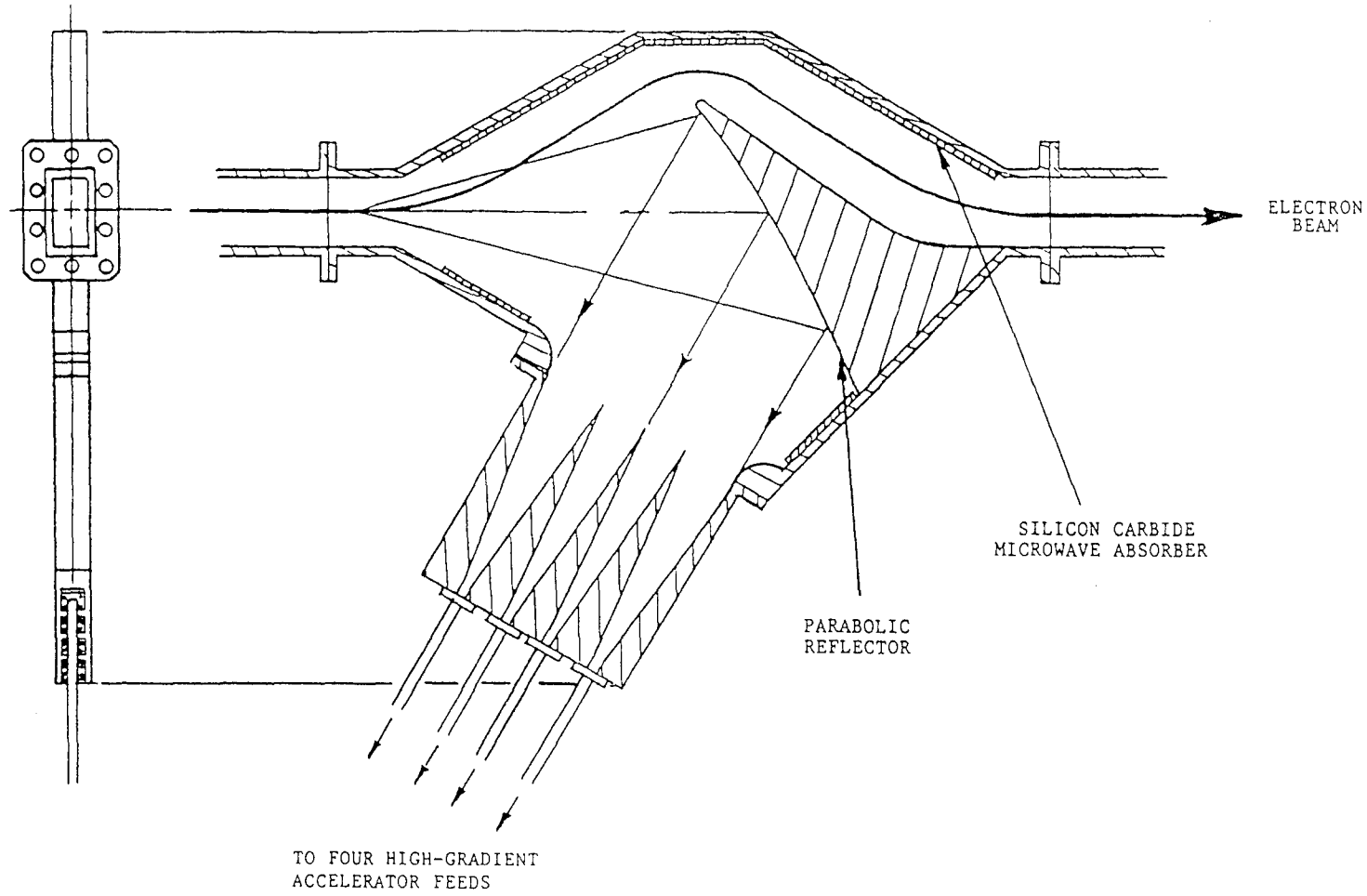

XBL 893-855

Fig. 2b

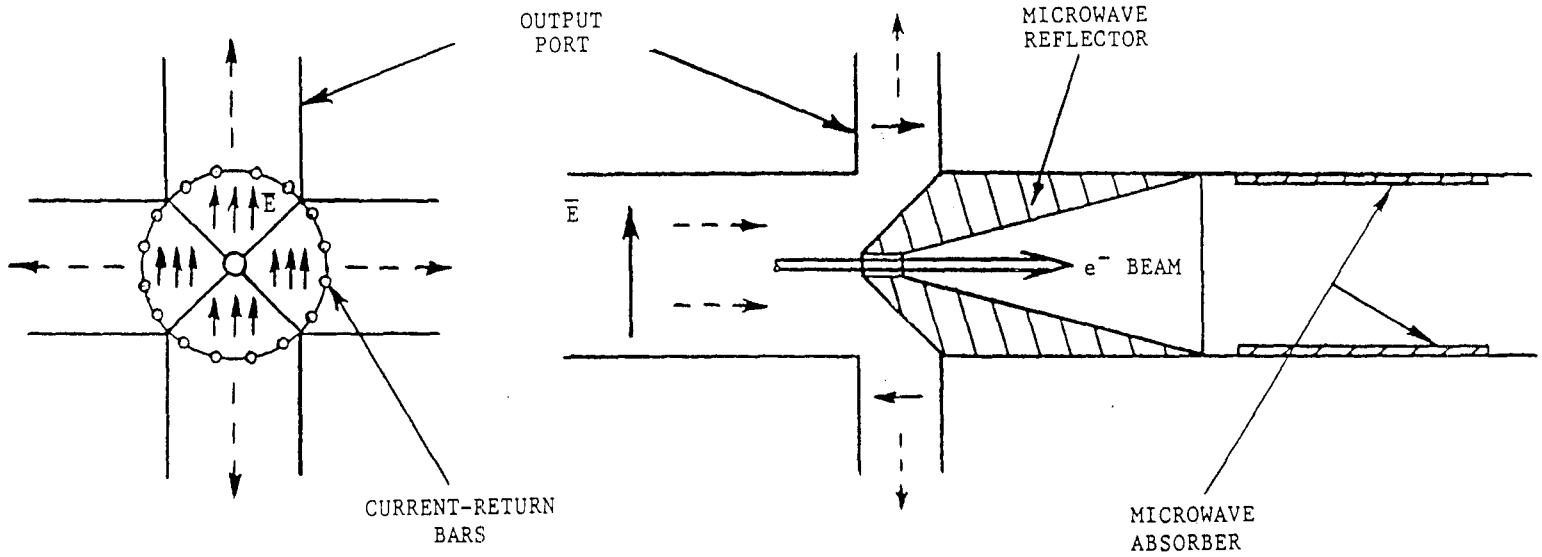

XBL 893-869

Fig. 2c

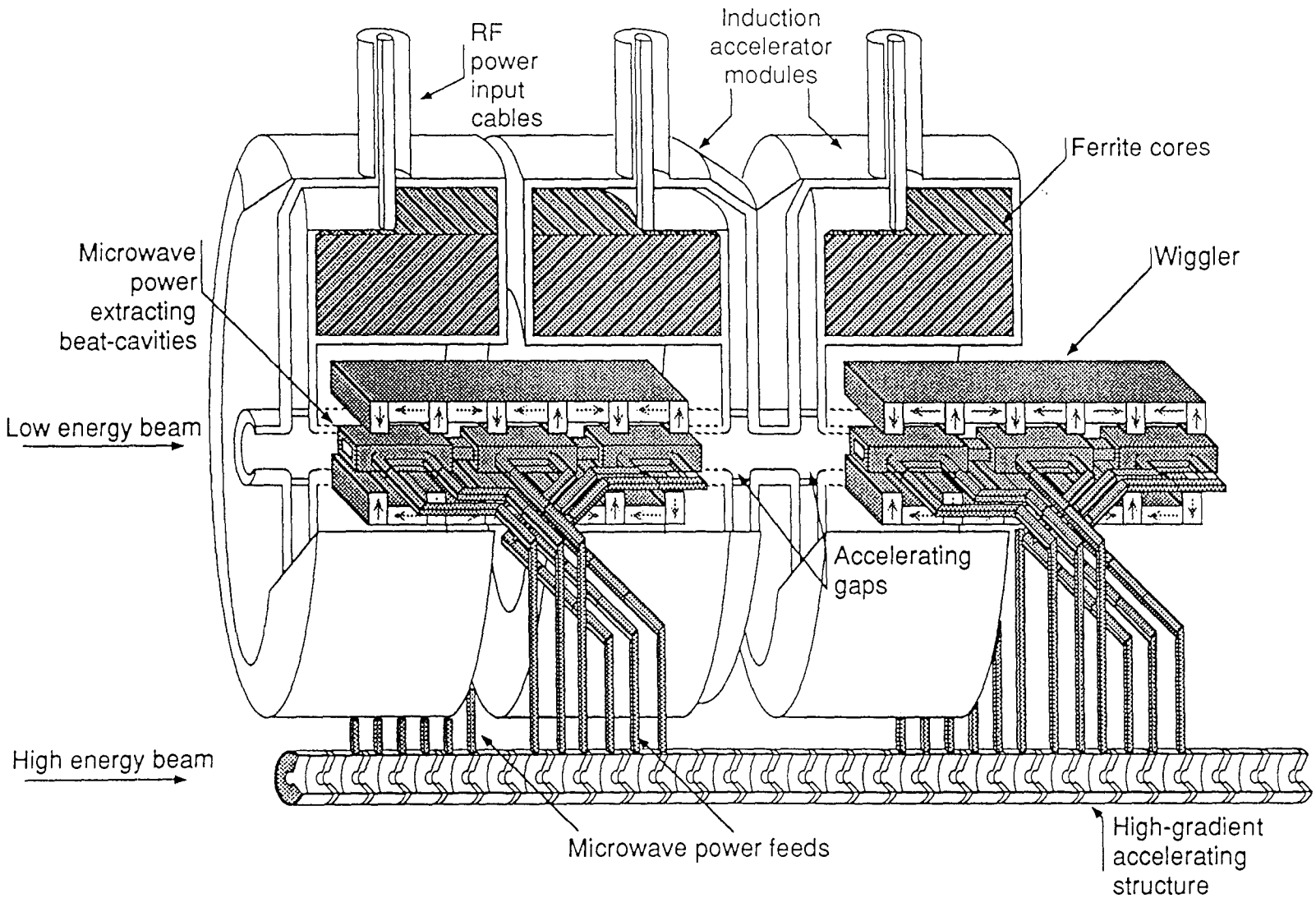
RF
power
input
cables
Induction
accelerator
modules
Ferrite cores
Microwave
power
extracting
beat-cavities
Wiggler
Low energy beam
Accelerating
gaps
High energy beam
Microwave power feeds
High-gradient
accelerating
structure

Fig. 3

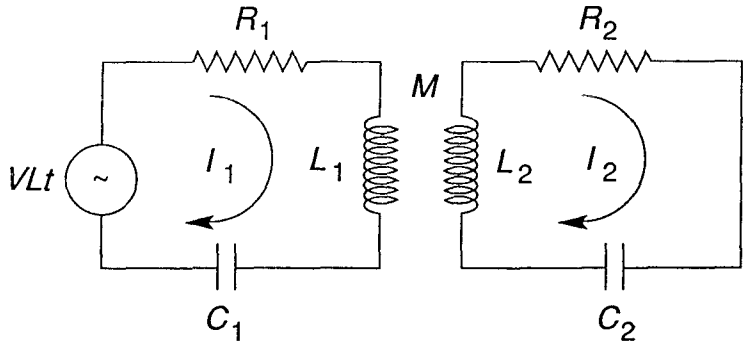

XBL 9010-5572a

Fig. 4

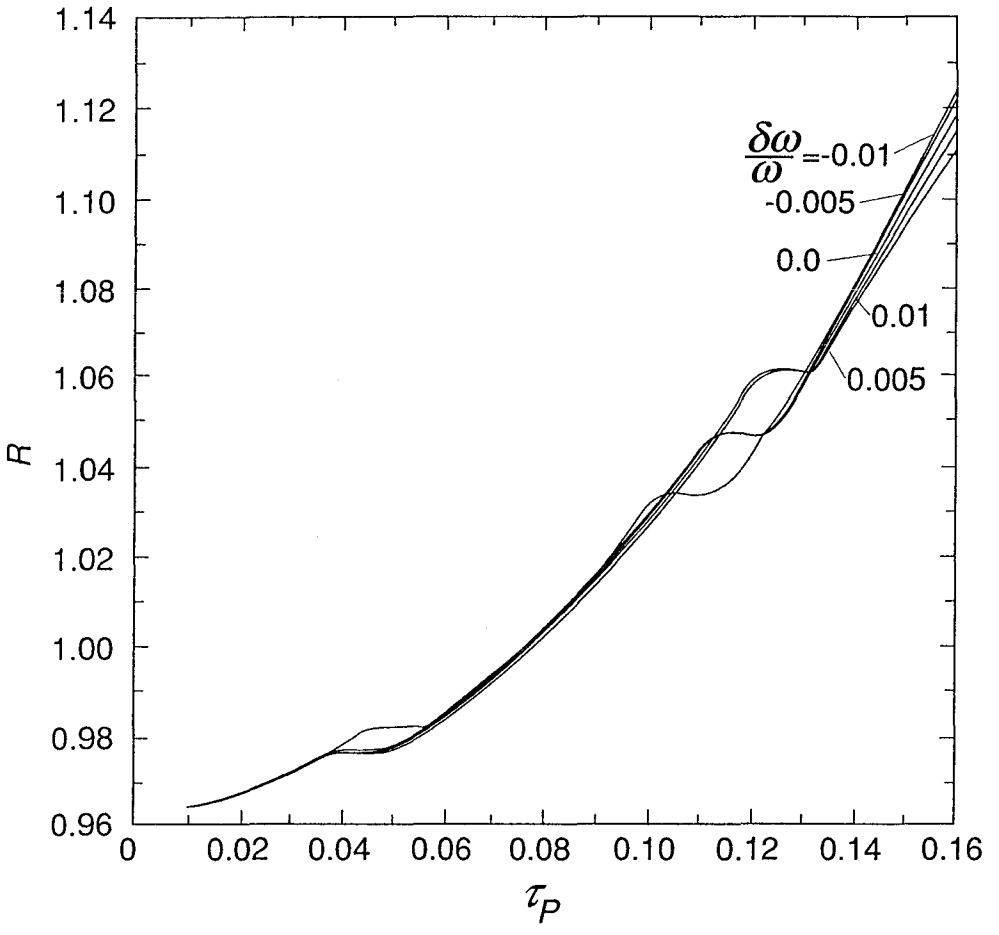

XBL 9010-5573a

Fig. 5

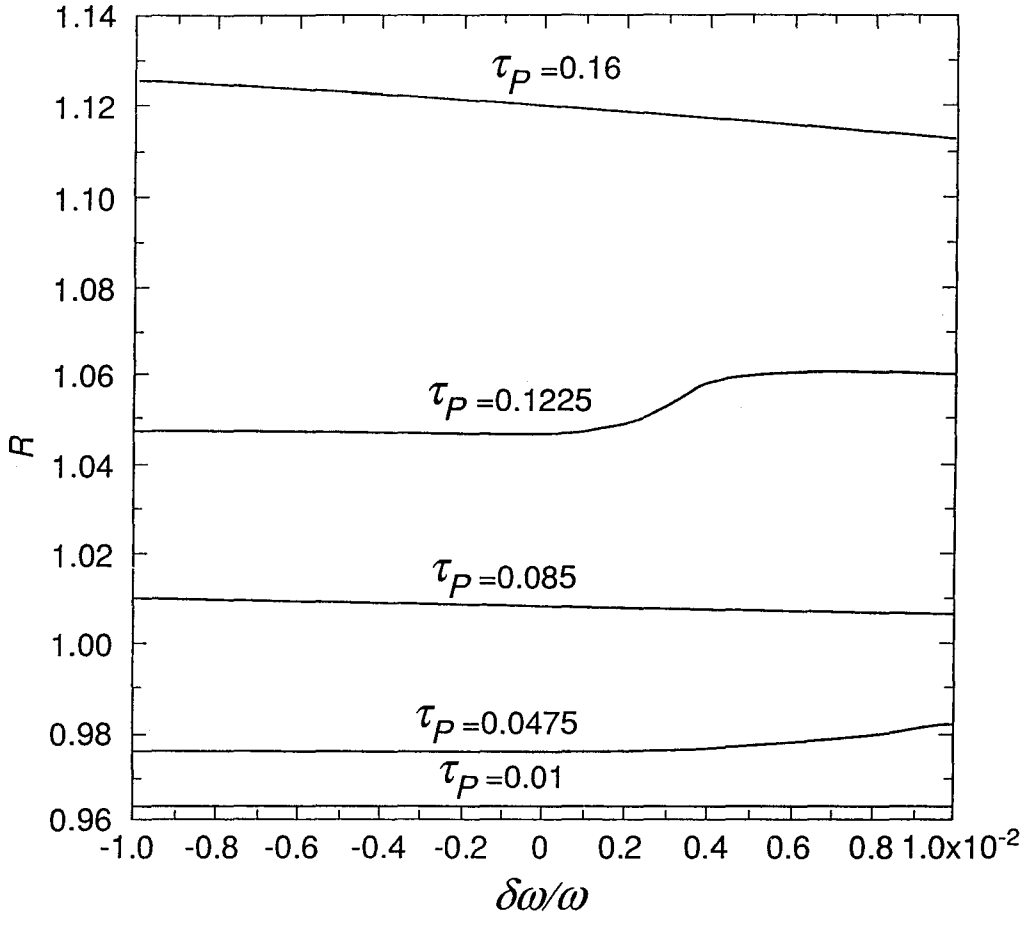

XBL 9010-5574a

Fig. 6

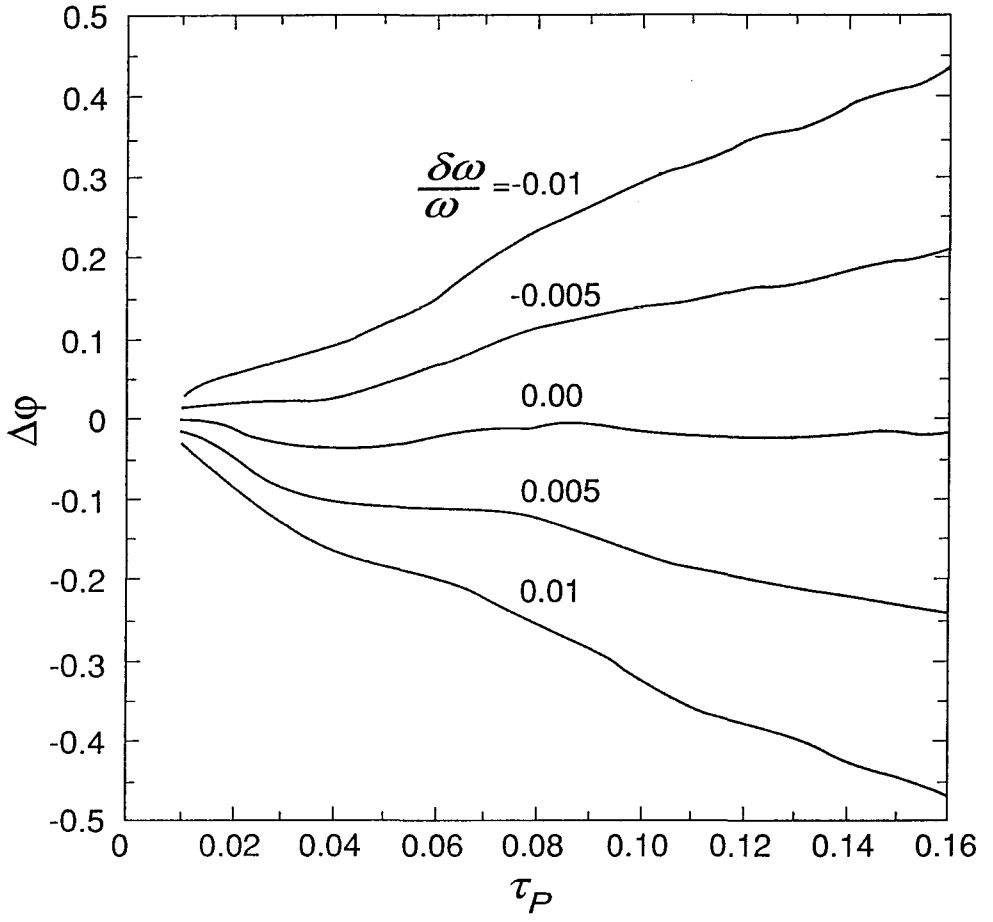

XBL 9010-5575b

Fig. 7

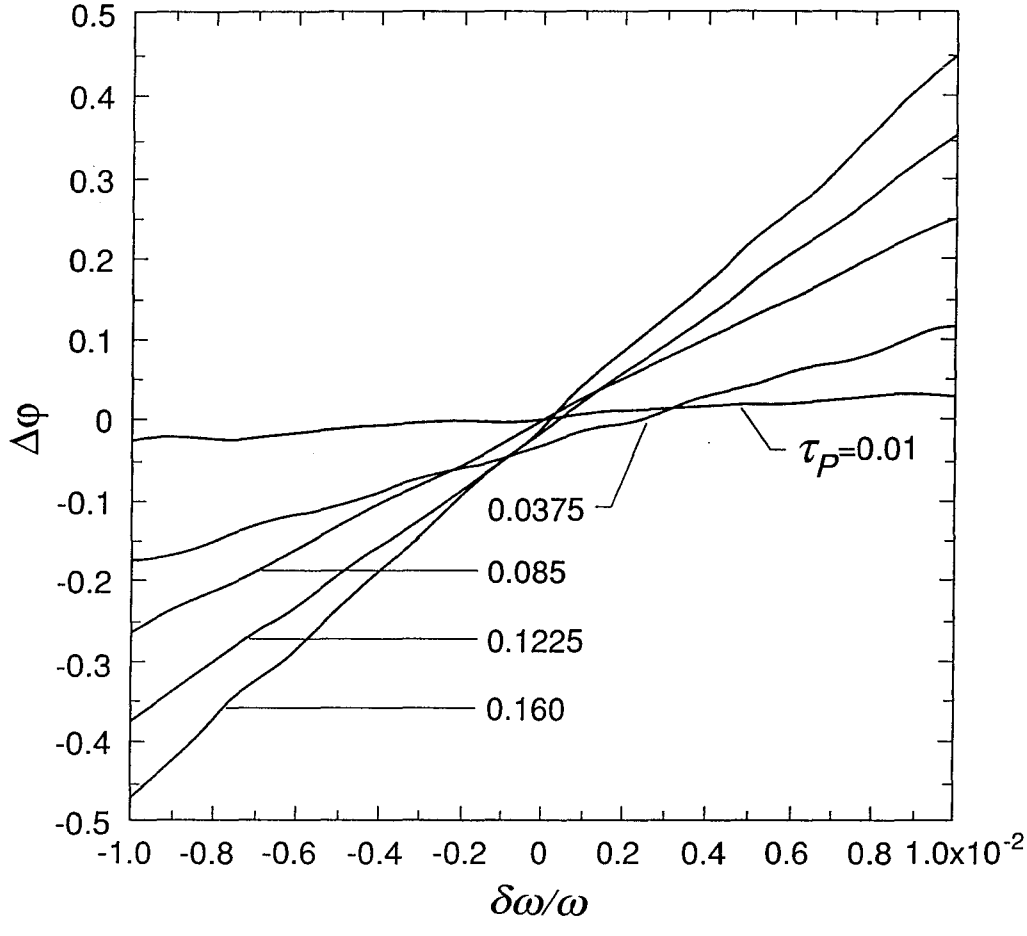

XBL 9010-5576b

Fig. 8

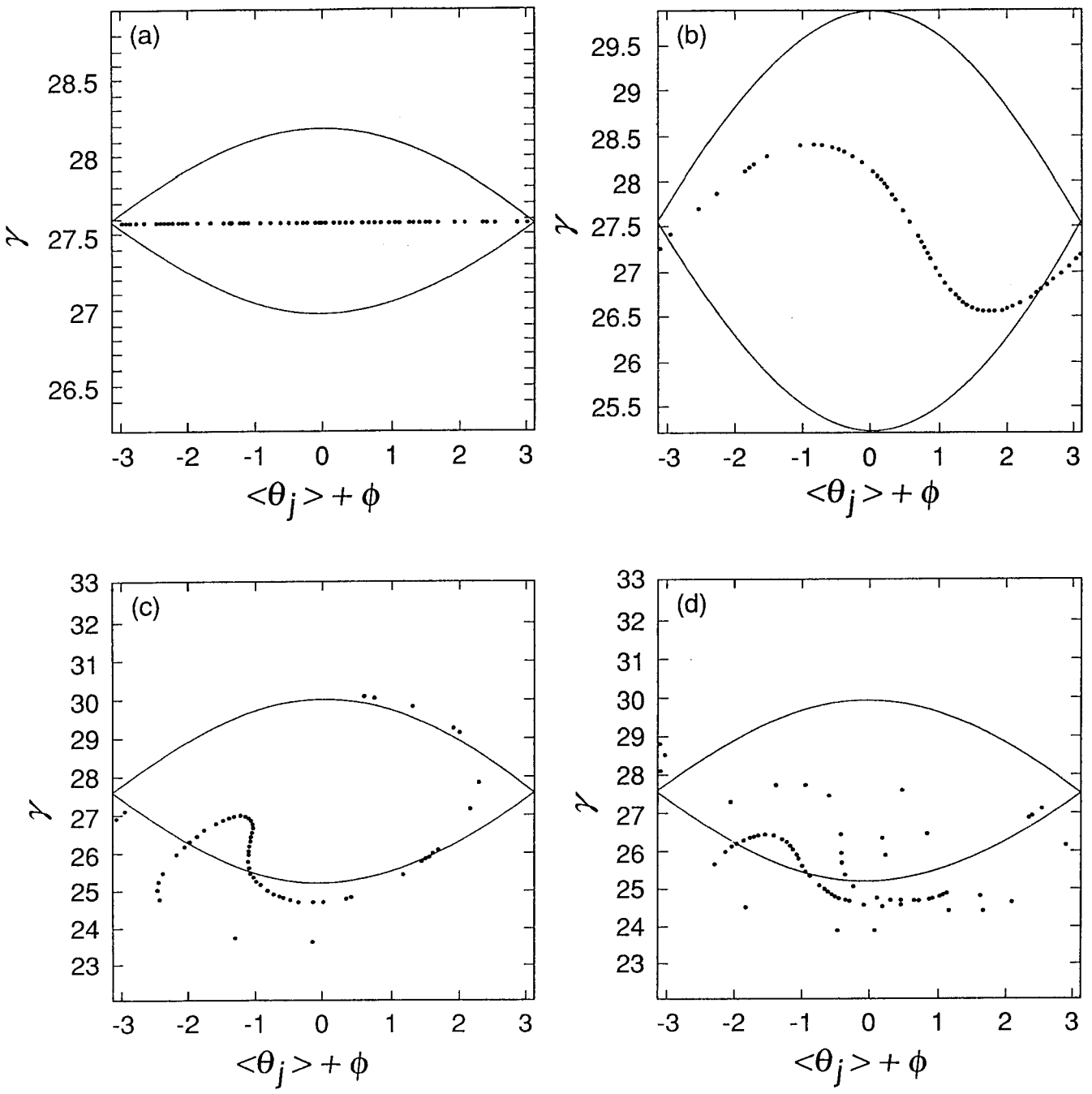

Fig. 9

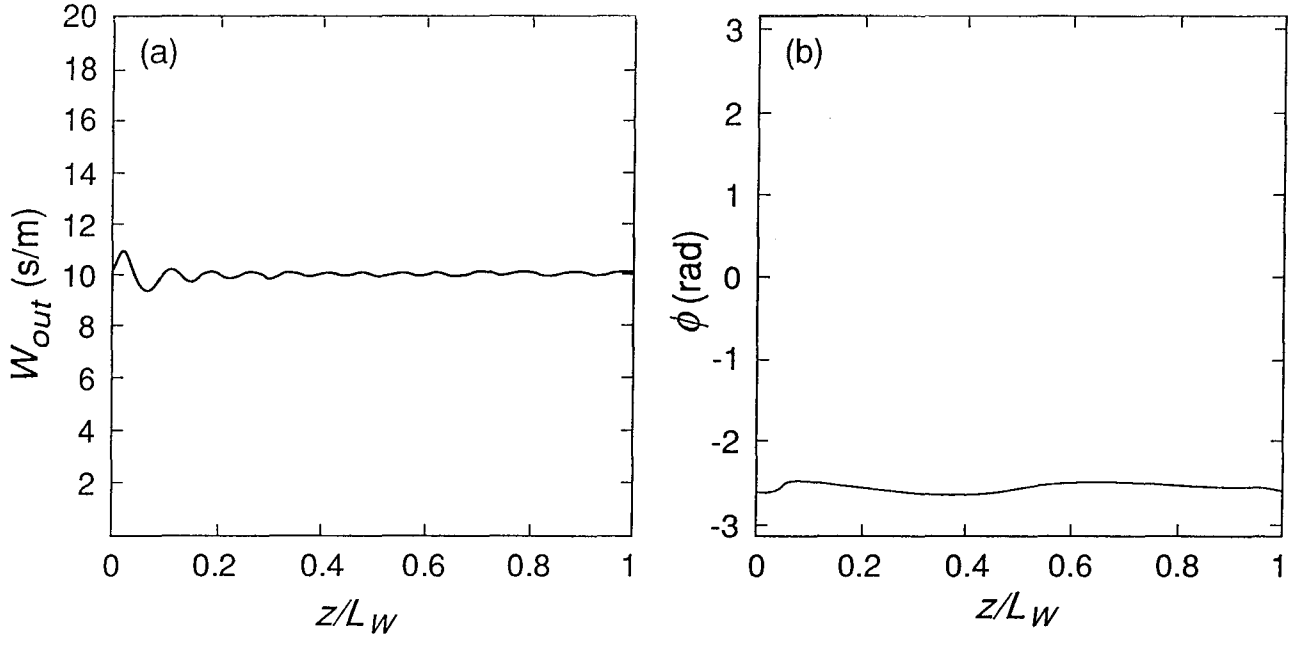

XBL 9010-5578a

Fig. 10

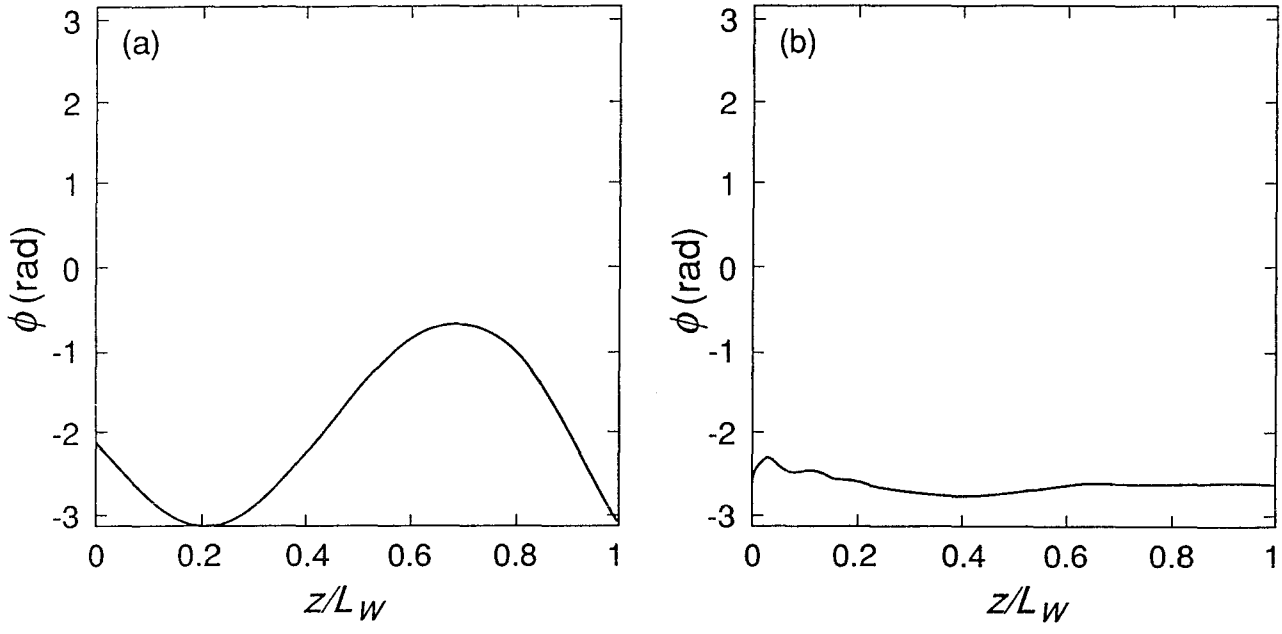

XBL 9010-5579a

Fig. 11

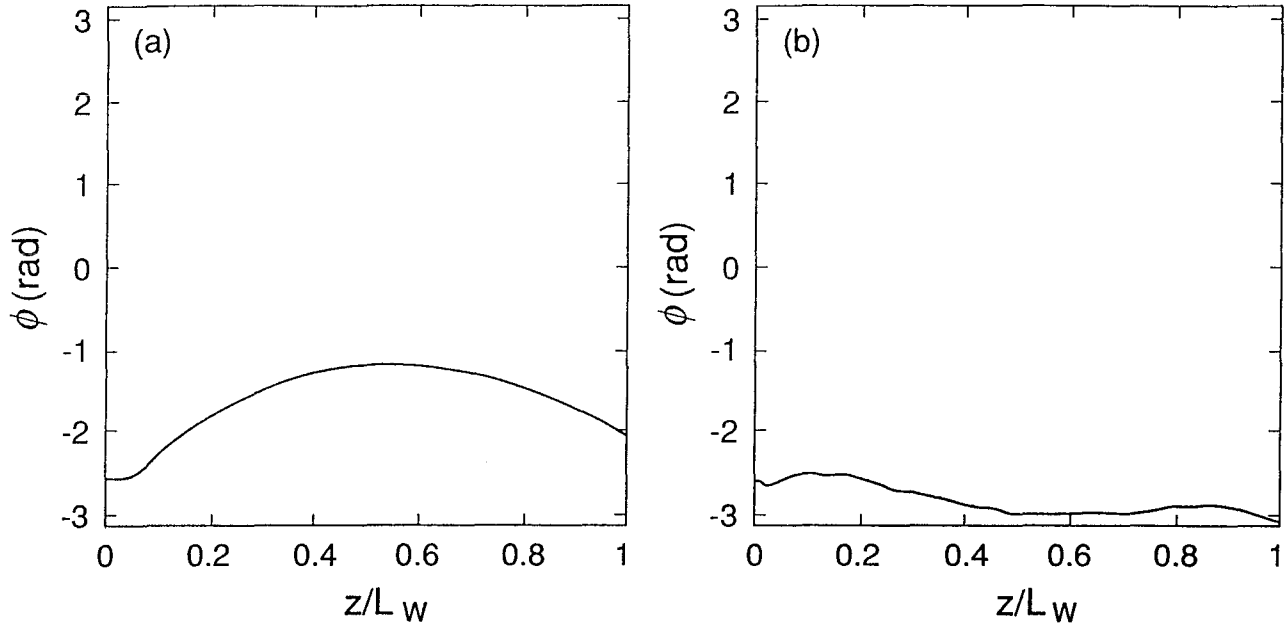

XBL 9010-5580a

Fig. 12